Dynamic ^{68}Ga-DOTATATE PET/MRI in the Diagnosis and Management of Intracranial Meningiomas

Jana Ivanidze
Weill Cornell Medical College: Weill Cornell Medicine
Michelle Roytman
NewYork-Presbyterian Hospital/Weill Cornell Medical Center
Myrto Skafida
NewYork-Presbyterian Hospital/Weill Cornell Medical Center
Sean Kim
Weill Cornell Medical College: Weill Cornell Medicine
Shannon Glynn
Weill Cornell Medical College: Weill Cornell Medicine
Joseph R. Osborne
NewYork-Presbyterian Hospital/Weill Cornell Medical Center
Susan C. Pannullo
NewYork-Presbyterian Hospital/Weill Cornell Medical Center
Eaton Lin
NewYork-Presbyterian Hospital/Weill Cornell Medical Center
Nicolas A Karakatsanis (nak2032@med.cornell.edu)
Weill Cornell Medical College, Cornell University https://orcid.org/0000-0001-7326-3053

Original research

Keywords: DOTATATE, PET, Dynamic, Patlak, Meningioma, post-treatment change

Posted Date: December 1st, 2020

DOI: https://doi.org/10.21203/rs.3.rs-116183/v1

Version of Record: A version of this preprint was published at Radiology: Imaging Cancer on March 1st, 2022. See the published version at https://doi.org/10.1148/rycan.210067.

Abstract

Background: While MRI is the gold standard for meningioma diagnosis and treatment planning, it poses limitations in differentiating residual/recurrent disease from post-treatment-change. ^{68}Ga-DOTATATE PET/MR of 50 min with standardized uptake value (SUV) analysis has demonstrated clinical utility in patients with meningioma. However, SUV is considered semi-quantitative with limited reproducibility depending on several variable parameters not accounted for in its definition. Dynamic PET acquisitions enable parametric imaging accounting for post-injection time to improve quantification. Our purpose was to assess feasibility and clinical utility of dynamic ^{68}Ga-DOTATATE PET/MR with multi-parametric SUV and Patlak analysis in the diagnosis and management of intracranial meningioma.

Results: 19 subjects with meningioma underwent dynamic ^{68}Ga-DOTATATE PET/MR. Time-activity curves were generated in 84 volumes of interest (53 meningioma, 9 post-treatment-change, 22 cranial blood pool reference in superior sagittal sinus, SSS). Region-specific net binding rate constant *Ki* was determined using the standard and generalized Patlak (sPatlak and gPatlak) methods with a population-based reference input function. Absolute and relative mean and maximum SUVs were extracted from the 50 minutes (SUV_{50}) and the last 10 minutes (SUV_{10}) of acquisition. Spearman correlation, Mann-Whitney, and Wilcoxon tests were performed. In meningioma, absolute and relative maximum SUV_{50} demonstrated a strong, significant, positive correlation with sPatlak *Ki* ($r = 0.82$, $p < 0.0001$ and $r = 0.85$, $p < 0.0001$, respectively). Similar results were found in post-treatment-change regions ($r = 0.88$, $p = 0.007$ and $r = 0.83$, $p = 0.015$, respectively). Mean SUV_{50} demonstrated similar correlations with sPatlak *Ki* in both subgroups. No significant differences were observed between sPatlak and gPatlak *Ki* correlations with SUV. All SUV and *Ki* metrics were significantly higher in meningioma versus post-treatment-change regions. SUV_{50} and SUV_{10} metrics for each sub-cohort were not significantly different. No lesions were reclassified based on SUV_{10} or *Ki* compared to SUV_{50}.

Conclusions: Multi-parametric SUV and Patlak *Ki* analysis with ^{68}Ga-DOTATATE PET/MR is feasible and can differentiate meningioma from post-treatment-change. *Ki* may improve quantification of postoperative residual/ recurrent meningioma. SUV_{10} and SUV_{50} yielded comparable quantification suggesting feasibility for shorter PET scans.

Trial Registration Number (ClinicalTrials.gov ID): NCT04081701, Registration Date: September 9, 2019

Background

Meningiomas are the most common primary intracranial tumors, accounting for nearly 40% of all primary brain tumors and over 50% of non-malignant tumors[1]. The World Health Organization (WHO) classifies meningioma into three grades with a total of 15 subtypes[2]. Approximately 80% of cases are benign (WHO grade I) and carry a favorable prognosis, however, grade II and III meningiomas are associated with increased rates of recurrence and associated 5-year-survival rates of 78% and 44%, respectively[3]. Contrast-enhanced magnetic resonance imaging (MRI) is the gold standard for treatment planning and

post-operative evaluation of meningiomas; however, MRI has its limitations discerning recurrent/residual disease from post-operative findings (*3*), often requiring multiple follow-up examinations to differentiate the two entities, which may result in a delay in diagnosis with an associated potential increase in morbidity and mortality. Furthermore, MRI can have limited accuracy in cases of infiltrative or “en plaque” lesions, as well as in the setting of osseous or parenchymal invasion.

Meningiomas express high levels of somatostatin receptor 2 (SSTR2)[4]. Given the lack of physiologic SSTR2 expression in the calvarium, meninges and brain parenchyma (with the exception of the pituitary gland), SSTR2 represents an attractive target for molecular imaging of meningiomas[4]. Positron emission tomography (PET) imaging with SSTR ligands has enabled the detection and delineation of meningiomas, particularly for radiation treatment planning[5, 6]. ^{68}Ga-DOTATATE binds to SSTR2 with high specificity as opposed to other somatostatin analogs used in SSTR-targeted molecular imaging[7, 8]. Its clinical utility has been demonstrated in the differentiation of meningioma and post-treatment change[9], as well as in the detection of transosseous meningiomas when compared to MRI[10, 11].

In the current clinical setting, meningioma PET/MR data is typically acquired in static mode, i.e. over a single time frame, to produce a single time snapshot of the radiotracer concentration averaged over a given scan time frame. While helpful in clinical practice, this method may be considered as semi-quantitative as it does not account for the dependence of the radiotracer-target interaction on several variable factors across exams, including the scan time window relative to injection and the radiotracer concentration in a background reference region[12, 13].

Dynamic PET instead allows for evaluation of the radiotracer kinetics over time in both tissue and blood plasma to improve tumor characterization and treatment response monitoring [12, 14-16]. The standard Patlak graphical analysis is a robust linear method commonly used for modeling of the irreversible or mildly reversible kinetics of radiotracers in dynamic PET[17]. The highly quantitative parameter of net utilization or binding rate constant, *Ki*, of the radiotracer in tissues can be determined from the slope of the Patlak plot after fitting to the linear model the extracted tissue and reference time-activity curves [17]. Whole-body (WB) Patlak PET imaging may attain superior lesion detectability and reduce false-positive rates when complementing standard-of-care SUV [15, 16].

As a receptor ligand, ^{68}Ga-DOTATATE is confined to tissues that express SSTR2, and for which the absolute quantification of ^{68}Ga-DOTATATE binding rate *Ki* may provide a more reproducible metric of SSTR2 expression compared to SUV alone. *Ki* has been shown to more accurately reflect tumor SSTR density than SUV in neuroendocrine tumors[18], noting a nonlinear relationship between *Ki* and SUV for high *Ki* values, attributed to faster blood clearance in patients with a high tumor receptor expression[18, 19]. We report the first investigation on the feasibility of dynamic ^{68}Ga-DOTATATE PET/MRI brain scans followed by combined multi-parametric SUV and Patlak *Ki* analysis and their clinical utility in the diagnosis and treatment response assessment of meningioma.

Methods

Patients

Institutional review board approval with waived consent was obtained for this retrospective, HIPAA compliant study. A total of 19 subjects with 40 target lesions participated in this study. Each subject underwent a PET/MRI examination as part of an observational pilot cohort (Table 1). Through clinical chart review, demographic and clinical information was recorded for all patients including age at diagnosis, sex, WHO stage of meningioma at time of pathological diagnosis, and surgical and/or radiation treatment history.

Image Acquisition and Reconstruction

PET/MRI was performed on the Biograph mMR scanner (Siemens Healthineers, Erlangen, Germany) or the GE SIGNA PET/MR scanner (GE Healthcare, Milwaukee, WI). Subjects were injected with on average 172.9 MBq of ^{68}Ga-DOTATATE (SD: 18.4 MBq). A dynamic list-mode 3D PET data acquisition of 50 minutes was initiated within 5-15 minutes post injection (p.i.). The PET list data from the entire 50-minute scan period as well as from the last 10 minutes of acquisition were binned into two respective static data frames. In addition, the list data were binned into 10 sequential post injection (p.i.) frames of 5 minutes each. All static and dynamic PET frames were subsequently reconstructed with the standard Ordered-Subset Expectation-Maximization (OS-EM) algorithm using 3 iterations and 21 (Siemens Biograph mMR) or 28 (GE Signa) subsets of projection views. An image matrix size of 344 x 344 x 127 (192 x 192 x 89) voxels with each voxel having a size of 2.086 x 2.086 x 2.031 (1.875 x 1.875 x 2.780) mm^3 were employed for the Siemens Biograph mMR (GE Signa) PET image reconstructions.

MRI was performed according to institutional protocol, including pre- and post-contrast sagittal 3D T1 SPACE (TR/TE 600–700 ms/11-19 ms, 120-degree flip,1 mm slice thickness) and 3D T2 FLAIR (TR/TE 6300–8500ms/394-446 ms, 120-degree flip, 1 mm slice thickness). MR-based PET attenuation correction was obtained according to manufacturer's standard-of-care specifications. In 2 of the subjects, dynamic PET/CT was acquired instead of PET/MR due to patient-specific contraindications to 3 Tesla MRI, and the PET images were aligned and fused to recent contrast-enhanced MRI of the same subjects utilizing Syngo.via software (Siemens Healthineers, Erlangen, Germany).

Regions Evaluation

Volumes of interest (VOIs) were delineated in targeted regions across all the dynamic PET images using Vinci (Max Planck Institute for Metabolism Research, Cologne, Germany)[20]. The VOIs were drawn for selected lesions including meningioma (radiographically suspected and/or pathologically proven), suspected post-treatment-change, and superior sagittal sinus (SSS, as an approximation of background cranial blood pool, according to previously published methodology, negative reference)[9]. Tumors with a diameter larger than 0.6 cm and with high tracer avidity (determined visually) were included for evaluation. The anatomical delineation of the VOIs in the PET images was based on the co-registered sagittal 3D T1 post-contrast MR images with respective axial and coronal reformations.

Of the total 19 PET datasets, an expert observer drew VOIs on VINCI for 14 scans while another drew VOIs for the other 8 scans. In addition, to evaluate inter-observer agreement on VOIs delineation, both experts drew VOIs from a common subset of 5 PET datasets, randomly selected from the study sample, in 12 unique regions including 7 meningiomas, and 5 superior sagittal sinus (SSS).

Static Analysis and Post-Injection Acquisition Window

Absolute maximum and mean SUV values were extracted at each targeted VOI from the entire 50-minute acquisition window (SUV_{50}) and the last 10 minutes of acquisition (SUV_{10}). In addition, the extracted SUVs were normalized to the respective SUVs of the SSS region to yield the relative maximum and mean SUV scores for each acquisition window.

Kinetic Analysis

Time-activity curves (TACs) data were extracted in mean kBq/ml units from the delineated VOIs across all the dynamic PET images. Injection on the scanner table was not possible for the PET/MR scans due to the lack of an MR-compatible portable injection shield needed to ensure minimal radiation exposure for the staff during injection. Thus, all PET/MR scans commenced at 5 to 15 minute p.i.. A population-based reference SSS TAC model was employed to infer the missing 5 to 15 minutes of SSS TAC data needed by the Patlak method to quantify the *Ki* parameter for each region. In particular, a full 0 - 60 minutes p.i. reference SSS TAC model was built from image-derived SSS TACs extracted from a separate cohort of ^{68}Ga-DOTATATE PET/CT scans starting concurrently with injection on the scanner table. The 0-60 minutes reference SSS TAC model was then fitted to the 50-minute SSS reference TAC, as extracted from each PET/MR exam, to infer the missing TAC data from the first 5 to 15 minutes p.i. [21].

The standard Patlak (sPatlak) and generalized Patlak (gPatlak) graphical analysis methods were employed for the kinetic analysis of the dynamic PET TACs data and the estimation of the net utilization or binding rate constant *Ki* parameter for each target VOI[17, 22]. The sPatlak method assumes an irreversible binding process for ^{68}Ga-DOTATATE and is highly robust as it involves a simple linear regression fit. The gPatlak method is a more general method that employs with the additional parameter of net efflux rate constant k_{loss} and a non-linear regression fit to account for a mild degree of ^{68}Ga-DOTATATE reversible binding in tissue when estimating *Ki*[22]. The target and reference VOI TACs were then combined according to the assumptions of the respective Patlak method to form the sPatlak and gPatlak plots.

Subsequently, the data of each plot were fitted using the Ordinary Least Squares (OLS) linear regression method[23] for the sPatlak and the Basis Function Method (BFM)[22] for the gPatlak method. The slope of each fit yielded the respective sPatlak *Ki* (*sKi*) and gPatlak *Ki* (*gKi*) scores for each VOI. The two Patlak plots and the respective fitting processes were implemented in Matlab (Natick, MA, USA) platform. Finally, the *Ki* features of the ^{68}Ga-DOTATATE in the brain were visually assessed by performing the robust

sPatlak analysis on a voxel-by-voxel basis across the entire field-of-view to produce *sKi* images of the whole brain of each subject.

Statistical Analysis

Spearman analyses were performed to assess correlation between *Ki* and maximum or mean SUV_{50} in meningioma and post-treatment-change regions. To evaluate differences in Spearman correlations between *sKi* vs. SUV and *gKi* vs. SUV, we also calculated a z-score and p-value for each different type of SUV metric[24]. Mann-Whitney tests were also employed to assess statistical significance in the score differences between meningioma and post-treatment-change lesions for the metrics of SUV, *sKi* and *gKi*. Additionally, Wilcoxon tests were performed to determine the statistical significance in the differences between SUV_{50} and SUV_{10} scores. To assess for interobserver variability, interclass correlation coefficients (ICC) estimates and 95% confidence intervals (CI) were calculated from the 12 common VOIs of the inter-observer subgroup of studies using SPSS statistical package version 26 (SPSS Inc., Chicago, IL) based on the mean-rating (k = 2), absolute and consistency-agreement, 2-way mixed-effects models [25]. In all statistical tests above, the significance level was set to a p value of less than 0.05 (Prism, version 6.07; GraphPad Software, Inc.).

Results

Study Population

Dynamic ^{68}Ga-DOTATATE PET/MRI was performed on 19 patients (6 male and 13 female; mean age 63.2 years, range: 36-81years) with a history of clinically suspected or pathology-proven meningioma (WHO-I, N=4; WHO-II, N=9; WHO-III, N=2; Presumed, N=4) with a total of 53 meningiomas and 9 regions of suspected post-treatment change. The clinical and demographic characteristics of the study population are presented in Table 1.

Dynamic PET/MR acquisition and multi-parametric image analysis

Figure 1 demonstrates ^{68}Ga-DOTATATE PET dynamic images from an early, mid- and late-frame as well as the respective PET images fused with T1 post-contrast MRI in a representative subject. Figure 2 demonstrates a ^{68}Ga-DOTATATE SUV_{50} image compared to a standard Patlak *Ki* image for the same subject before and after fusion with a T1 post-contrast MR image.

Comparison of Post-Injection Acquisition Window

A side-by-side comparison of ^{68}Ga-DOTATATE PET SUV_{50} and SUV_{10} images fused with T1-postcontrast MR is presented in Figure 3. In Figure 4, we assessed the distribution of absolute and relative maximum SUV_{50} and SUV_{10} scores in meningioma and post-treatment-change regions. Statistically significant differences were observed between SUV_{50} and SUV_{10} metrics for both absolute and relative scores (p-value < 0.0001). However, SUV_{50} and SUV_{10} metrics were not significantly different for each subcohort.

Furthermore, the SUV lesion/SSS ratio cut-off value of 3, which was previously established for maximum SUV_{50} scores[9], did not result in reclassification of any lesions when SUV_{10} scores were used instead. Thus, shorter 10 min scan periods may be sufficient in clinical practice for accurate SUV-based stratification of lesions into recurrent meningioma versus post-treatment change.

Comparison of SUV and Patlak-derived *Ki* values

Ki values estimated from the sPatlak and gPatlak graphical analysis methods were calculated for all VOIs as described in the methods section. In total, 53 meningiomas and 9 VOIs consistent with post-treatment change were included in the study. In meningioma, absolute and relative maximum SUV_{50} demonstrated a strong, significant, positive correlation with *sKi* ($r = 0.82$, $p < 0.0001$ and $r = 0.85$, $p < 0.0001$, respectively). Similar results were found in post-treatment-change regions ($r = 0.88$, $p = 0.007$ and $r = 0.83$, $p = 0.015$, respectively). Similarly, absolute and relative maximum SUV_{50} demonstrated a strong, significant, positive correlation with *gKi* in meningiomas ($r = 0.77$, $p < 0.0001$ and $r = 0.81$, $p < 0.0001$, respectively), and post-treatment-change regions ($r = 0.90$, $p = 0.0046$ and $r = 0.81$, $p = 0.0218$, respectively). Moreover, mean absolute and relative SUV_{50} demonstrated similarly positive and strong correlations with *sKi* and *gKi* in both meningioma and post-treatment-change regions (Table 2). To compare Spearman correlations of *sKi* and *gKi* with SUV, respectively, a z-score statistic and p-value were generated for each pair[24]. None of these p-values were significant (Table 2).

Differentiation of meningioma from post-treatment change

We further investigated the clinical utility of maximum SUV_{50}, maximum SUV_{10}, *sKi* and *gKi*, in differentiating meningioma from post-treatment change. Our analysis identified statistically significant differences between meningioma and post-treatment-change regions for all mean and maximum SUV (Figure 4) and *sKi* and *gKi* (Figure 5) (Table 3). In Figure 6, the differences in the Patlak plots for meningioma vs. post-treatment change regions are demonstrated under both sPatlak and gPatlak model assumptions. Stratification into meningioma versus post-treatment-change lesions based on absolute or relative SUV_{50} or SUV_{10} was not affected when using *sKi* or *gKi* metrics instead.

Interobserver Variability

Intraclass correlation coefficients (ICC) comparing the *sKi* values from the meningioma between the two independent observers were 0.973 (95% CI: 0.853-0.995) and 0.970 (95% CI: 0.827-0.995) for the absolute and consistency agreement models, respectively.

Discussion

Sensitivity and specificity of contrast-enhanced MRI in meningioma can be limited in the post-surgical and post-radiation setting. PET/CT and PET/MR imaging with somatostatin analogs has demonstrated utility in delineating tumor volumes, particularly prior to radiation therapy. DOTATATE PET/MRI was previously shown to improve assessment for recurrent/ residual tumor, particularly in patients in whom

tumor location limits gross total resection, and patients with WHO-II/-III disease[9]. Furthermore, postoperative SSTR-targeted PET may improve residual tumor detection rates compared to intraoperative Simpson grading[26].

Dynamic ^{18}F-FDG PET has been shown to improve lesion detectability in oncologic imaging, with superior lesion contrast and decreased false-positive rates[13, 15]. Dynamic ^{68}Ga-DOTATATE PET in meningioma has hitherto not been explored. Compared to SUV metrics alone, the direct estimation of Patlak *Ki* regional scores accounts both for the reference dynamic uptake in SSS and for the dynamic trend of ^{68}Ga-DOTATATE in the tissues of interest. Thus, regional Patlak *Ki* analysis can provide a more quantitative and reproducible metric of SSTR2 expression in meningiomas vs post-treatment-change regions regardless of the post injection scan time window. Moreover, Patlak analysis permits more quantitative comparisons between scans, e.g. between pre- and post-treatment to assess response, as it is less dependent on the activity distribution in the blood or other negative reference regions, such as the SSS[12]. By complementing SUV with absolute *Ki* scores additional physiologic information can be extracted to improve understanding of the pathophysiology, as well as to achieve higher lesion detectability, especially in terms of specificity and reproducibility between scans[15].

In this study, we employed the standard linear Patlak graphical analysis method to quantify *Ki* under the assumptions of irreversible ^{68}Ga-DOTATATE SSTR2 binding. The more generalized non-linear Patlak method was also evaluated to account for any potential mild degree of reversible binding rate of ^{68}Ga-DOTATATE[22]. However, no statistically significant difference in the differentiation of meningioma from post-treatment-change was observed between the two Patlak methods (Figure 5). Our findings favor the use of the sPatlak over the gPatlak model in future ^{68}Ga-DOTATATE PET/MR meningioma studies, as the former offers a relatively more robust and simplified method for *Ki* quantification[21].

Our findings support a role for dynamic ^{68}Ga-DOTATATE PET/MRI in meningioma evaluation. We found a strong significant positive correlation between *Ki* and SUV in meningioma and post-treatment-change cohorts, suggesting early and sustained binding of SSTR2 on meningiomas. Moreover, ICC analysis demonstrated that *Ki* values can be extracted with high inter-observer agreement, suggesting that the proposed approach is robust and reproducible with potential for adaptation into clinical practice.

We also compared the SUV scores from the static ^{68}Ga-DOTATATE images of the last 10 minutes (SUV_{10}) versus SUV scores from the entire 50-minute acquisition period (SUV_{50}). Given that the SUV_{50} and SUV_{10} metrics were not significantly different for each subcohort, our data suggests that static acquisition could be considerably shortened to 10 min without losing significant information, an important benefit for PET/CT scans or pediatric subjects. However for simultaneous PET/MR studies where the MR sequences often last more than 30 minutes, the availability of long scan periods may be exploited to perform similarly long dynamic PET scans parallel to the MR, thus enabling multi-parametric 68Ga-DOTATATE imaging[12].

In this study, we focused on brain scans, as systemic metastatic disease would not be expected with WHO-I and -II meningioma. However, our current study findings can serve as a pilot to expand the current scope to whole-body dynamic ^{68}Ga-DOTATATE PET scans and multi-parametric SUV/*Ki* analysis[23] in neoplasms with systemic involvement such as metastatic esthesioneuroblastoma and paraganglioma. In addition, dynamic ^{68}Ga-DOTATATE PET/MRI may provide more reliable means of personalized treatment planning in meningioma patients, as well as improve dosimetry analysis in the targeted radiation therapy of meningioma with ^{177}Lu-DOTATATE[27, 28].

Limitations of our study include the lack of dynamic PET data in the first 5-15 minutes p.i., as we were not equipped with MR-compatible injection shields to allow injections inside the PET/MR scanner field-of-view. Nevertheless, we built a robust population-based reference ^{68}Ga-DOTATATE input function model. Moreover, longer PET acquisitions beyond the first 1 hour p.i. would be needed in future to determine the optimal scan time window for ^{68}Ga-DOTATATE meningioma studies.

Conclusions

The clinical feasibility of multi-parametric SUV and Patlak Ki 68Ga-DOTATATE PET/MR imaging and analysis for the diagnosis and management of meningioma patients was demonstrated in this study. The complement of semi-quantitative SUV images with highly reproducible Patlak Ki regional scores or images can enhance quantification and facilitate differentiation of meningioma from post-treatment effects. Finally, the last 10-min, as opposed to the entire 50 minutes, of PET data acquired simultaneously with MR during the first hour post injection may be adequate for the extraction of SUV scores with high contrast between meningioma and post-treatment-change regions.

Declarations

ACKNOWLEDGEMENTS

The authors would like to thank Ms. Gabriela Madera, research coordinator in the department of radiology at Weill Cornell Medicine, for her help in administrative aspects of this study.

Compliance with Ethical Standards

Funding: This study was internally funded; the authors disclose funding support from AAA/Novartis for an ongoing investigator initiated clinical trial building on these results.

Conflict of Interest: JI has been awarded a research grant from Advanced Accelerator Applications (AAA), a Novartis company. All other authors declare that they have no conflict of interest.

Ethical Approval: All procedures performed in studies involving human participants were in accordance with the ethical standards of the institutional and/or national research committee and with the 1964 Helsinki declaration and its later amendments or comparable ethical standards.

Informed consent: Informed consent was obtained from all individual participants included in the study.

References

1. Ostrom QT, Gittleman H, Liao P, Vecchione-Koval T, Wolinsky Y, Kruchko C, et al. CBTRUS Statistical Report: Primary brain and other central nervous system tumors diagnosed in the United States in 2010-2014. Neuro Oncol. 2017;19:v1-v88. doi:10.1093/neuonc/nox158.
2. Louis DN, Perry A, Reifenberger G, von Deimling A, Figarella-Branger D, Cavenee WK, et al. The 2016 World Health Organization Classification of Tumors of the Central Nervous System: a summary. Acta neuropathologica. 2016;131:803-20. doi:10.1007/s00401-016-1545-1.
3. Durand A, Labrousse F, Jouvet A, Bauchet L, Kalamarides M, Menei P, et al. WHO grade II and III meningiomas: a study of prognostic factors. J Neurooncol. 2009;95:367-75. doi:10.1007/s11060-009-9934-0.
4. Silva CB, Ongaratti BR, Trott G, Haag T, Ferreira NP, Leaes CG, et al. Expression of somatostatin receptors (SSTR1-SSTR5) in meningiomas and its clinicopathological significance. Int J Clin Exp Pathol. 2015;8:13185-92.
5. Stade F, Dittmar JO, Jakel O, Kratochwil C, Haberkorn U, Debus J, et al. Influence of (68)Ga-DOTATOC on sparing of normal tissue for radiation therapy of skull base meningioma: differential impact of photon and proton radiotherapy. Radiat Oncol. 2018;13:58. doi:10.1186/s13014-018-1008-z.
6. Thorwarth D, Henke G, Muller AC, Reimold M, Beyer T, Boss A, et al. Simultaneous 68Ga-DOTATOC-PET/MRI for IMRT treatment planning for meningioma: first experience. Int J Radiat Oncol Biol Phys. 2011;81:277-83. doi:S0360-3016(10)03698-9 [pii] 10.1016/j.ijrobp.2010.10.078.
7. Rachinger W, Stoecklein VM, Terpolilli NA, Haug AR, Ertl L, Poschl J, et al. Increased 68Ga-DOTATATE uptake in PET imaging discriminates meningioma and tumor-free tissue. J Nucl Med. 2015;56:347-53. doi:10.2967/jnumed.114.149120.
8. Reubi JC, Schar JC, Waser B, Wenger S, Heppeler A, Schmitt JS, et al. Affinity profiles for human somatostatin receptor subtypes SST1-SST5 of somatostatin radiotracers selected for scintigraphic and radiotherapeutic use. Eur J Nucl Med. 2000;27:273-82. doi:10.1007/s002590050034.
9. Ivanidze J, Roytman M, Lin E, Magge RS, Pisapia DJ, Liechty B, et al. Gallium-68 DOTATATE PET in the Evaluation of Intracranial Meningiomas. J Neuroimaging. 2019;29:650-6. doi:10.1111/jon.12632.
10. Kunz WG, Jungblut LM, Kazmierczak PM, Vettermann FJ, Bollenbacher A, Tonn JC, et al. Improved Detection of Transosseous Meningiomas Using (68)Ga-DOTATATE PET/CT Compared with Contrast-Enhanced MRI. J Nucl Med. 2017;58:1580-7. doi:10.2967/jnumed.117.191932.
11. Afshar-Oromieh A, Giesel FL, Linhart HG, Haberkorn U, Haufe S, Combs SE, et al. Detection of cranial meningiomas: comparison of (6)(8)Ga-DOTATOC PET/CT and contrast-enhanced MRI. Eur J Nucl Med Mol Imaging. 2012;39:1409-15. doi:10.1007/s00259-012-2155-3.
12. Zaidi H, Karakatsanis N. Towards enhanced PET quantification in clinical oncology. Br J Radiol. 2018;91:20170508. doi:10.1259/bjr.20170508.

13. Dimitrakopoulou-Strauss A, Pan L, Sachpekidis C. Kinetic modeling and parametric imaging with dynamic PET for oncological applications: general considerations, current clinical applications, and future perspectives. Eur J Nucl Med Mol Imaging. 2020. doi:10.1007/s00259-020-04843-6.
14. Sachpekidis C, Hillengass J, Goldschmidt H, Wagner B, Haberkorn U, Kopka K, et al. Treatment response evaluation with (18)F-FDG PET/CT and (18)F-NaF PET/CT in multiple myeloma patients undergoing high-dose chemotherapy and autologous stem cell transplantation. Eur J Nucl Med Mol Imaging. 2017;44:50-62. doi:10.1007/s00259-016-3502-6.
15. Fahrni G, Karakatsanis NA, Di Domenicantonio G, Garibotto V, Zaidi H. Does whole-body Patlak (18)F-FDG PET imaging improve lesion detectability in clinical oncology? Eur Radiol. 2019;29:4812-21. doi:10.1007/s00330-018-5966-1.
16. Karakatsanis NA, Lodge MA, Tahari AK, Zhou Y, Wahl RL, Rahmim A. Dynamic whole-body PET parametric imaging: I. Concept, acquisition protocol optimization and clinical application. Phys Med Biol. 2013;58:7391-418. doi:10.1088/0031-9155/58/20/7391.
17. Patlak CS, Blasberg RG. Graphical evaluation of blood-to-brain transfer constants from multiple-time uptake data. Generalizations. J Cereb Blood Flow Metab. 1985;5:584-90. doi:10.1038/jcbfm.1985.87.
18. Thuillier P, Bourhis D, Karakatsanis N, Schick U, Metges JP, Salaun PY, et al. Diagnostic performance of a whole-body dynamic 68GA-DOTATOC PET/CT acquisition to differentiate physiological uptake of pancreatic uncinate process from pancreatic neuroendocrine tumor. Medicine. 2020;99:e20021. doi:10.1097/MD.0000000000020021.
19. Ilan E, Velikyan I, Sandstrom M, Sundin A, Lubberink M. Tumor-to-Blood Ratio for Assessment of Somatostatin Receptor Density in Neuroendocrine Tumors Using (68)Ga-DOTATOC and (68)Ga-DOTATATE. J Nucl Med. 2020;61:217-21. doi:10.2967/jnumed.119.228072.
20. Vollmar SC, J.; Sué, M.; Klein, J.; Jacobs, A.H. and Herholz, K. VINCI-volume imaging in neurological research, co-registration and ROIs included. . Forschung und wissenschaftliches Rechnen. 2003;114:115-31.
21. Karakatsanis NA, Casey ME, Lodge MA, Rahmim A, Zaidi H. Whole-body direct 4D parametric PET imaging employing nested generalized Patlak expectation-maximization reconstruction. Phys Med Biol. 2016;61:5456-85. doi:10.1088/0031-9155/61/15/5456.
22. Karakatsanis NA, Zhou Y, Lodge MA, Casey ME, Wahl RL, Zaidi H, et al. Generalized whole-body Patlak parametric imaging for enhanced quantification in clinical PET. Phys Med Biol. 2015;60:8643-73. doi:10.1088/0031-9155/60/22/8643.
23. Karakatsanis NA, Lodge MA, Zhou Y, Wahl RL, Rahmim A. Dynamic whole-body PET parametric imaging: II. Task-oriented statistical estimation. Phys Med Biol. 2013;58:7419-45. doi:10.1088/0031-9155/58/20/7419.
24. Soper DS. Significance of the Difference between Two Correlations Calculator https://www.danielsoper.com/statcalc. . 2020.
25. Koo TK, Li MY. A Guideline of Selecting and Reporting Intraclass Correlation Coefficients for Reliability Research. J Chiropr Med. 2016;15:155-63. doi:10.1016/j.jcm.2016.02.012.

26. Ueberschaer M, Vettermann FJ, Forbrig R, Unterrainer M, Siller S, Biczok AM, et al. Simpson Grade Revisited - Intraoperative Estimation of the Extent of Resection in Meningiomas Versus Postoperative Somatostatin Receptor Positron Emission Tomography/Computed Tomography and Magnetic Resonance Imaging. Neurosurgery. 2020. doi:10.1093/neuros/nyaa333.
27. Seystahl K, Stoecklein V, Schuller U, Rushing E, Nicolas G, Schafer N, et al. Somatostatin receptor-targeted radionuclide therapy for progressive meningioma: benefit linked to 68Ga-DOTATATE/-TOC uptake. Neuro Oncol. 2016;18:1538-47. doi:10.1093/neuonc/now060.
28. Makis W, McCann K, McEwan AJ. Rhabdoid papillary meningioma treated with 177Lu DOTATATE PRRT. Clin Nucl Med. 2015;40:237-40. doi:10.1097/RLU.0000000000000669.

Tables

TABLE 1. Clinical and demographic characteristics of the study population. Shown are clinical and demographic characteristics including patient age, sex, number of meningiomas identified, surgical and radiation treatment history, as well as pathology data where applicable. N = number; F = female; WHO = World Health Organization; SRS = stereotactic radiosurgery; RT = radiation therapy.

TABLE 1. Clinical characteristics of the study population	
N DOTATATE scans performed	19
Type of DOTATATE scan	17 PET/MR
	2 PET/CT
Patients with DOTATATE confirmed meningiomas	18/19 (one DOTATATE negative suggesting post-treatment change)
Age at diagnosis	63.3 (range 36-89)
Sex	68.4% F (13/19)
Volumes of Interest identified on DOTATATE PET	84
Meningioma	53
Post-treatment Change	9
Superior Saggital Sinus	19
N meningiomas per scan	5.2% (1/19) with 0 meningiomas
	52.6% (10/19) with 1 meningioma
	42.1% (8/19) with 2-4 meningiomas
	15.8% (3/19) with >4 meningiomas
	Median: 1.5 meningiomas per scan (range: 0-8)
WHO grade	21% (4/19) WHO grade unknown
	21% (4/19) WHO grade I
	47% (9/19) WHO grade II
	11% (2/19) WHO grade III
Surgical History	74% (14/19) prior resection
Radiation History	53% (10/19) radiation history
Radiation Therapy	60% (6/10) SRS
	10% (1/10) Cyber Knife
	10% (1/10) Gamma Knife
	10% (1/10) Proton beam
	10% (1/10) Multiple types of RT

TABLE 2. Spearman correlation analyses between SUV and *Ki* metrics. Shown are Spearman r and p-value, respectively, for absolute and relative mean and maximum SUV_{50} and SUV_{10}, correlated with *sKi* and *gKi*, respectively, for meningioma and post-treatment-change. To compare Spearman correlations of *sKi* and *gKi* with SUV, respectively, a z-score statistic and p-value was generated for each pair[24].

TABLE 2: SUV-Ki Correlations and their difference between sPatlak and gPatlak methods								
	Absolute SUV				**Relative SUV**			
Meningioma	**Max SUV_{50}**	**Max SUV_{10}**	**Mean SUV_{50}**	**Mean SUV_{10}**	**Max SUV_{50}**	**Max SUV_{10}**	**Mean SUV_{50}**	**Mean SUV_{10}**
***sKi*-SUV r**	0.82	0.80	0.78	0.79	0.85	0.84	0.78	0.90
***gKi*-SUV r**	0.77	0.74	0.72	0.70	0.81	0.79	0.78	0.86
z-score	0.68	0.74	0.69	1.02	0.65	0.75	0	0.89
p-value	0.49	0.46	0.49	0.31	0.51	0.45	1	0.37
	Absolute SUV				**Relative SUV**			
Post-Treatment-Change	**Max SUV_{50}**	**Max SUV_{10}**	**Mean SUV_{50}**	**Mean SUV_{10}**	**Max SUV_{50}**	**Max SUV_{10}**	**Mean SUV_{50}**	**Mean SUV_{10}**
sPatlak *Ki*-SUV r	0.88	0.79	0.79	0.86	0.83	0.81	0.93	0.93
gPatlak *Ki*-SUV r	0.90	0.79	0.79	0.88	0.81	0.81	0.95	0.95
z-score	-0.17	0	0	-0.14	0.11	0	-0.3	-0.3
p-value	0.87	1	1	0.89	0.92	1	0.76	0.76

TABLE 3. Mean SUV and Ki values in meningioma and post-treatment-change lesions. Mean values are given along standard error of the mean (in parentheses) with p-values resulting from Mann-Whitney tests comparing meningioma and post-treatment-change lesions for each parameter (illustrated in Figures 4 and 5).

TABLE 3: SUV and Ki scores and their differences between meningioma and post-treatment-change regions

	Absolute SUV			
	Max SUV_{50}	**Max SUV_{10}**	**Mean SUV_{50}**	**Mean SUV_{10}**
Meningioma	21.71 (3.09)	26.17 (3.61)	8.36 (1.24)	9.39 (1.35)
Post-Treatment-Change	1.33 (0.45)	1.71 (0.61)	0.77 (0.27)	0.78 (0.28)
p	<0.0001	<0.0001	<0.0001	<0.0001
	Relative SUV			
	Max SUV_{50}	**Max SUV_{10}**	**Mean SUV_{50}**	**Mean SUV_{10}**
Meningioma	17.59 (2.63)	21.75 (3.20)	10.94 (2.02)	13.64 (2.12)
Post-Treatment-Change	1.21 (0.49)	1.53 (0.62)	1.15 (0.39)	1.33 (0.43)
p	<0.0001	<0.0001	<0.0001	<0.0001
	sPatlak *Ki* (ml/min/g)		gPatlak *Ki* (ml/min/g)	
Meningioma	0.13 (0.03)		0.24 (0.06)	
Post-Treatment-Change	0.02 (0.01)		0.02 (0.01)	
p	0.0004		0.0006	

Figures

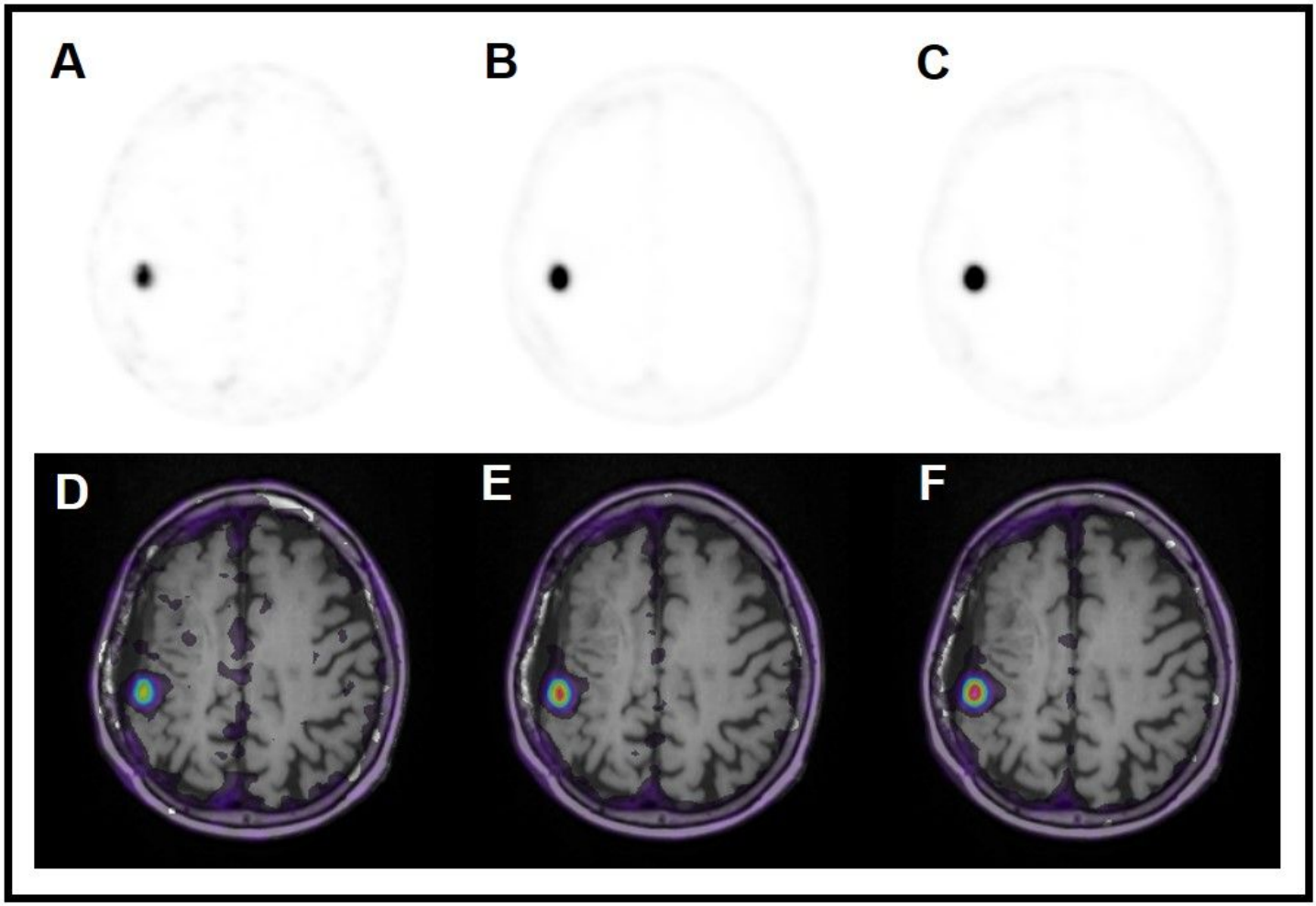

Figure 1

Axial 68Ga-DOTATATE PET dynamic images (A-C) and corresponding PET - T1 post-gadolinium fusion images (D-F) from 5-minute frames at 10 min p.i. (A, D), 30 min p.i. (B, E), and 45 min p.i. (C, F).

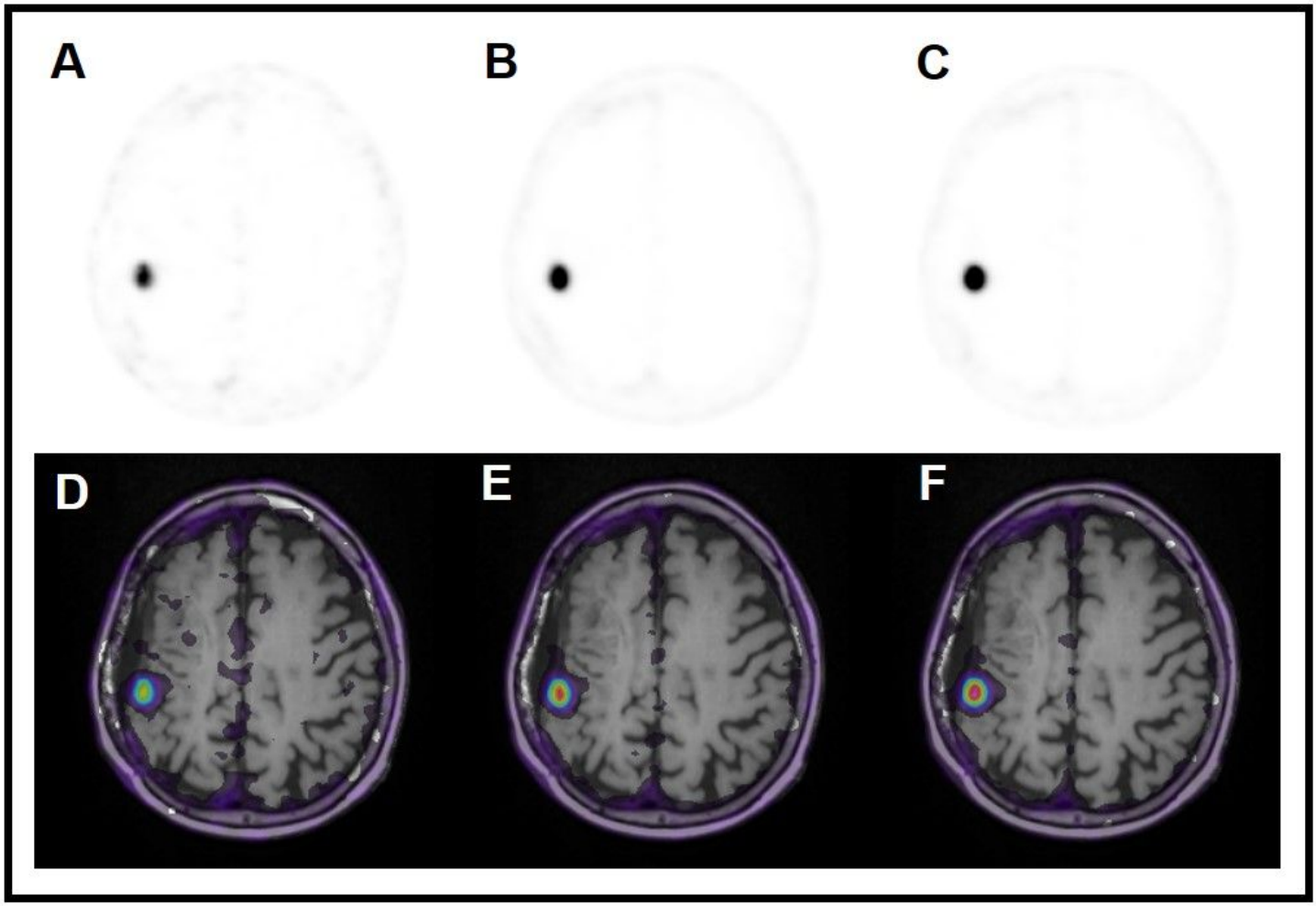

Figure 1

Axial 68Ga-DOTATATE PET dynamic images (A-C) and corresponding PET - T1 post-gadolinium fusion images (D-F) from 5-minute frames at 10 min p.i. (A, D), 30 min p.i. (B, E), and 45 min p.i. (C, F).

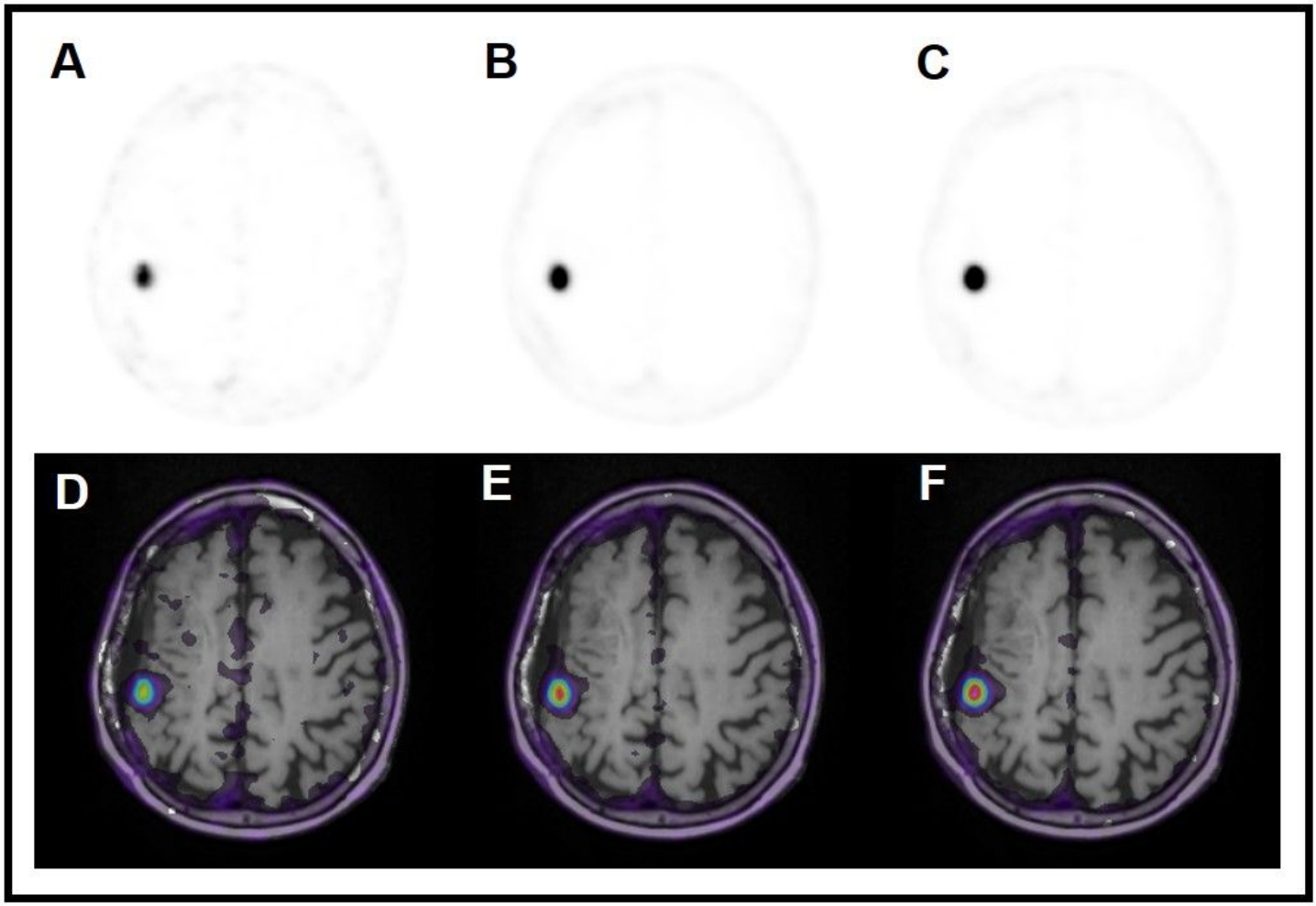

Figure 1

Axial 68Ga-DOTATATE PET dynamic images (A-C) and corresponding PET - T1 post-gadolinium fusion images (D-F) from 5-minute frames at 10 min p.i. (A, D), 30 min p.i. (B, E), and 45 min p.i. (C, F).

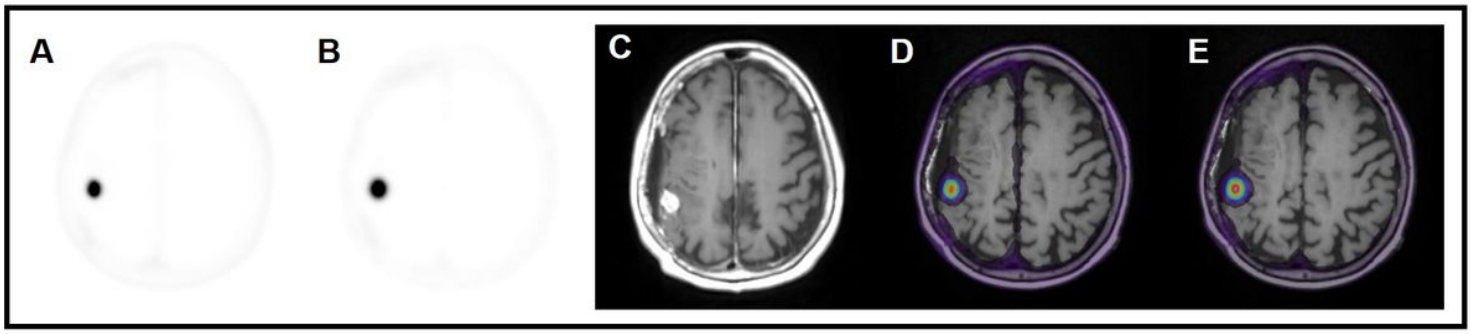

Figure 2

Axial images of 68Ga-DOTATATE PET SUV (A), Patlak Ki (B), 3D T1 post-gadolinium MR (C), fused PET SUV/MR T1 (D) and fused Patlak Ki/MR T1 (E) parameters from a single subject exam.

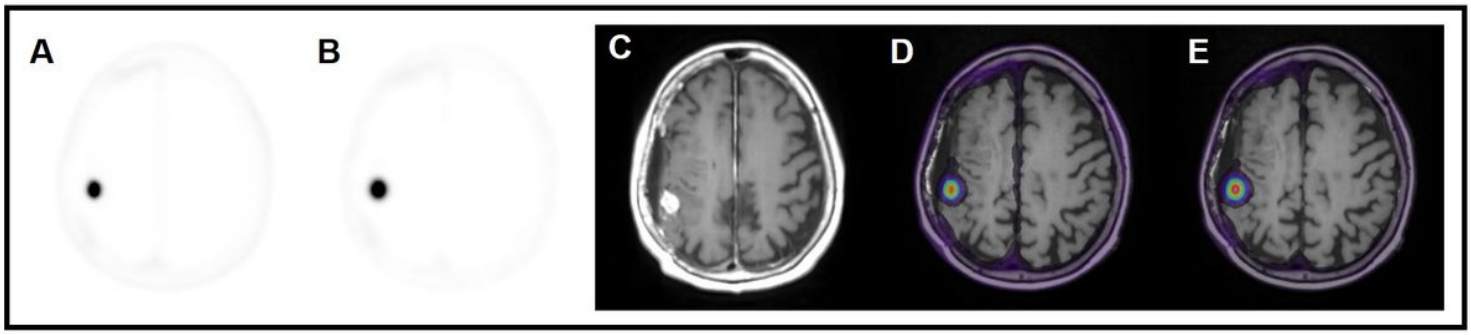

Figure 2

Axial images of 68Ga-DOTATATE PET SUV (A), Patlak Ki (B), 3D T1 post-gadolinium MR (C), fused PET SUV/MR T1 (D) and fused Patlak Ki/MR T1 (E) parameters from a single subject exam.

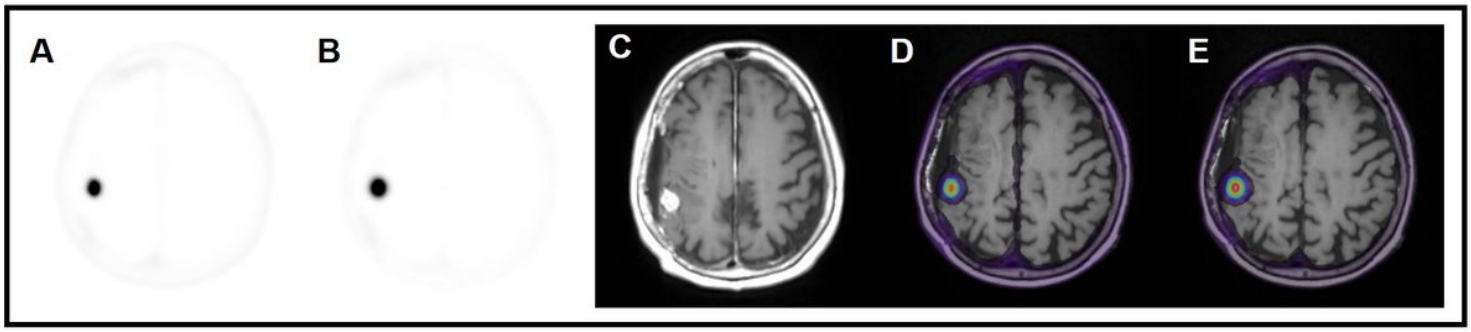

Figure 2

Axial images of 68Ga-DOTATATE PET SUV (A), Patlak Ki (B), 3D T1 post-gadolinium MR (C), fused PET SUV/MR T1 (D) and fused Patlak Ki/MR T1 (E) parameters from a single subject exam.

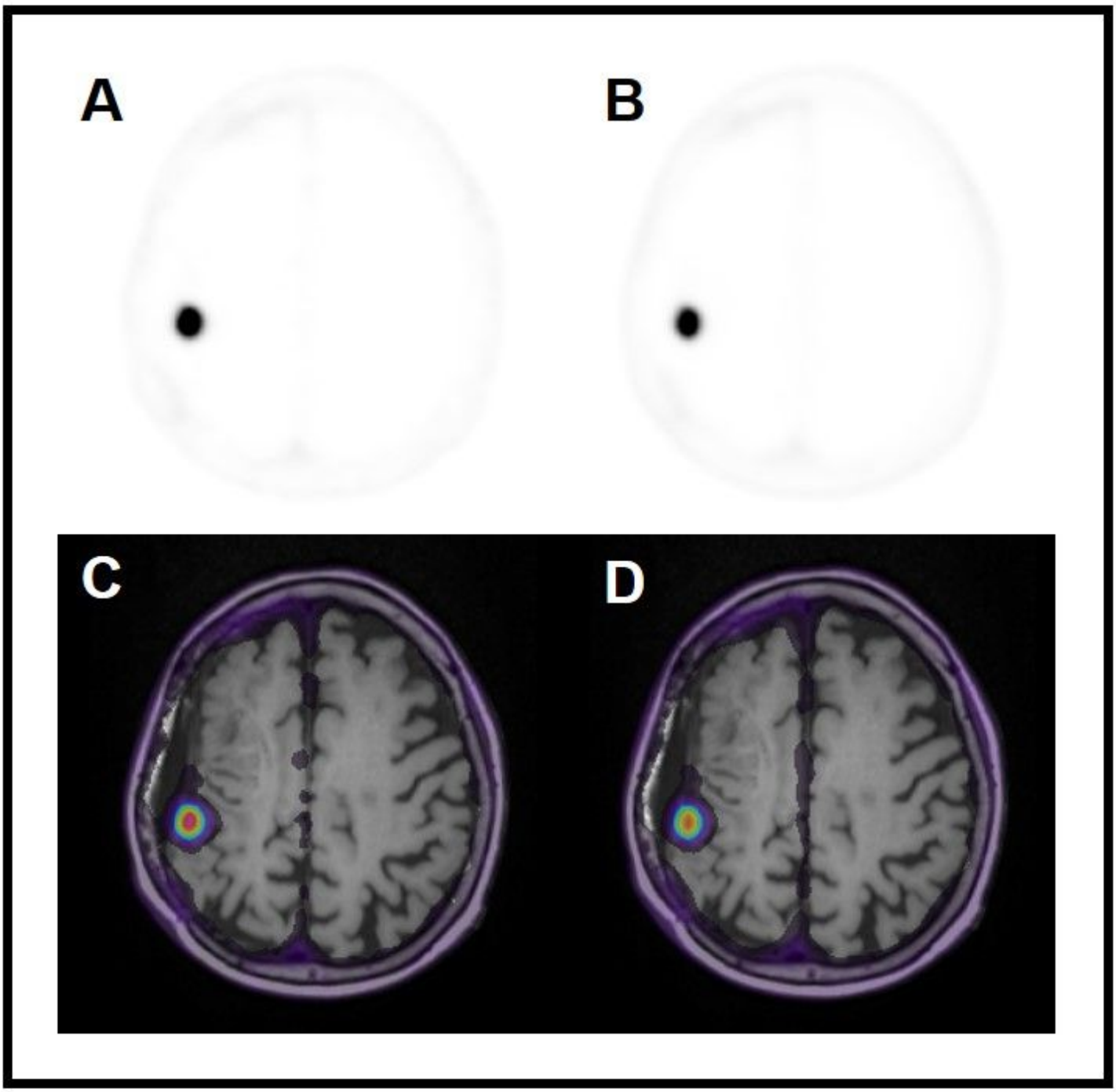

Figure 3

Axial 68Ga-DOTATATE PET images (A, B) and corresponding PET- T1 post-gadolinium fusion images (C-D) from the last 10-minutes frame at 50-60 min p.i. (A, C) and the entire 50-minutes scan at 10-60 min p.i. (B, D).

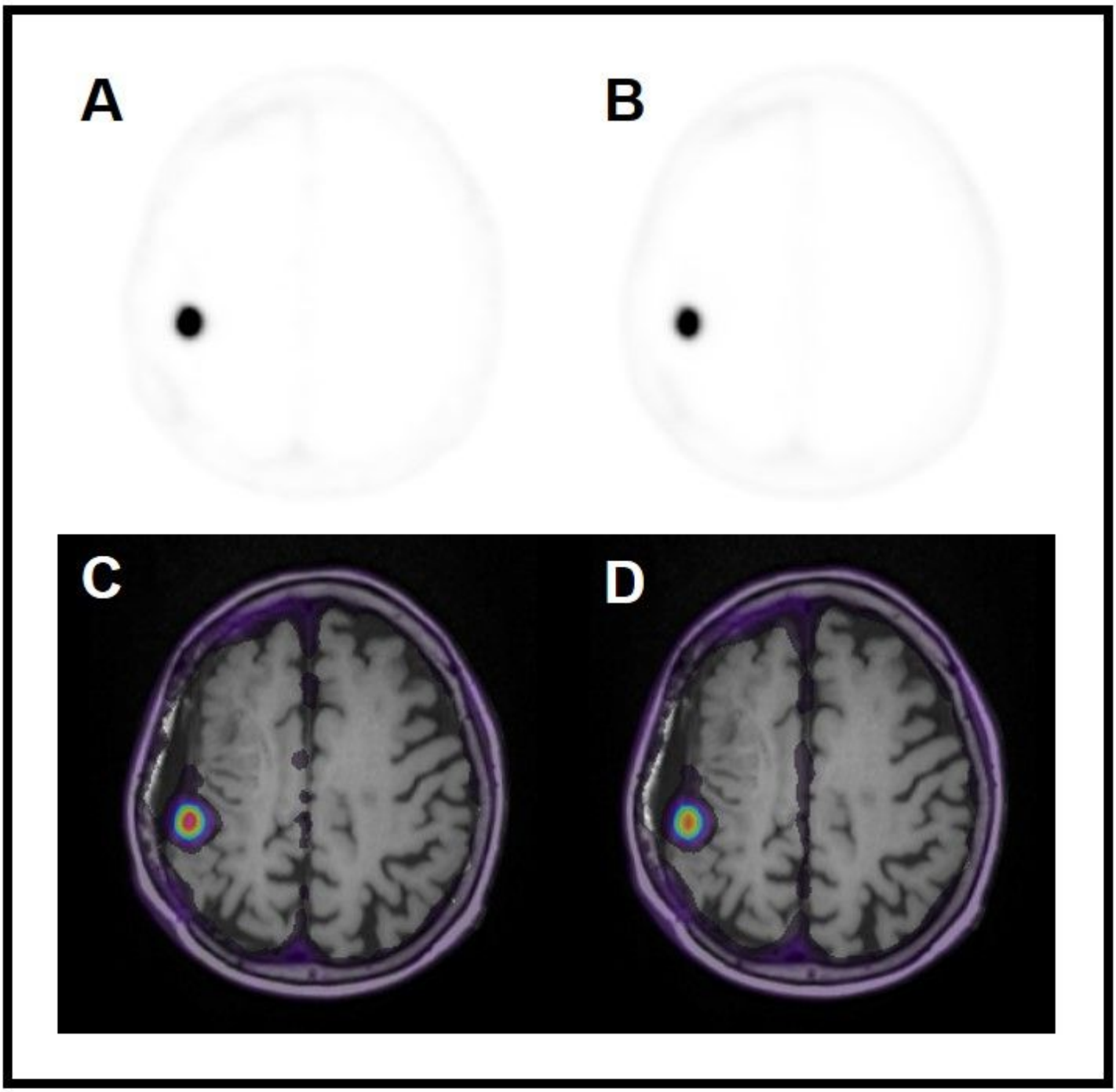

Figure 3

Axial 68Ga-DOTATATE PET images (A, B) and corresponding PET- T1 post-gadolinium fusion images (C-D) from the last 10-minutes frame at 50-60 min p.i. (A, C) and the entire 50-minutes scan at 10-60 min p.i. (B, D).

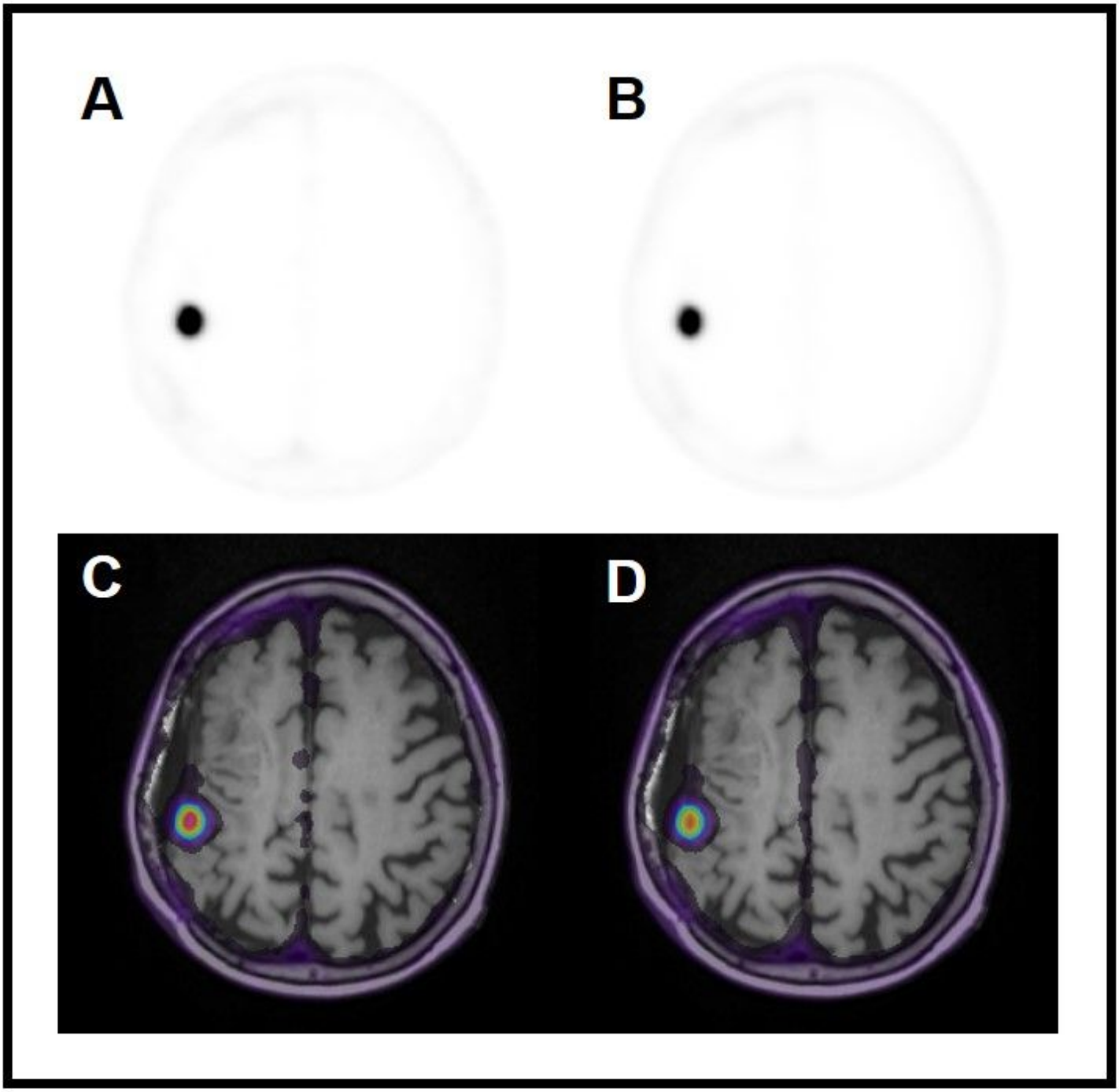

Figure 3

Axial 68Ga-DOTATATE PET images (A, B) and corresponding PET- T1 post-gadolinium fusion images (C-D) from the last 10-minutes frame at 50-60 min p.i. (A, C) and the entire 50-minutes scan at 10-60 min p.i. (B, D).

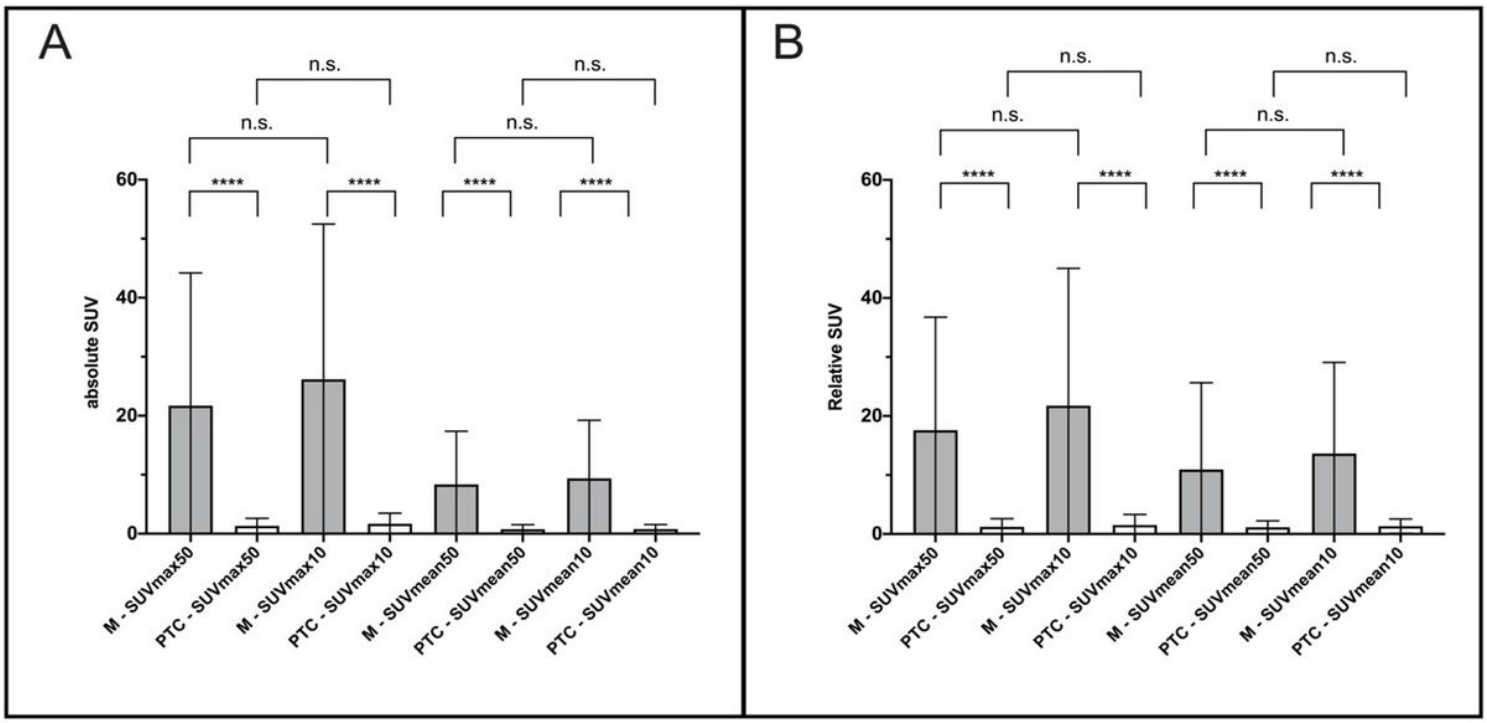

Figure 4

Comparison of meningioma (M, grey bars) and post-treatment-change lesions (PTC, white bars) using maximum and mean SUV acquired over the entire scan period (SUVmax50 and SUVmean50) and the last 10 minutes of acquisition (SUVmax10 and SUVmean10). Shown are mean and standard deviation. Figure 4A demonstrates absolute SUV; Figure 4B demonstrates relative SUV (normalized to the superior sagittal sinus, SSS). Asterisks indicate p-value (****, < 0.0001; n.s., not significant).

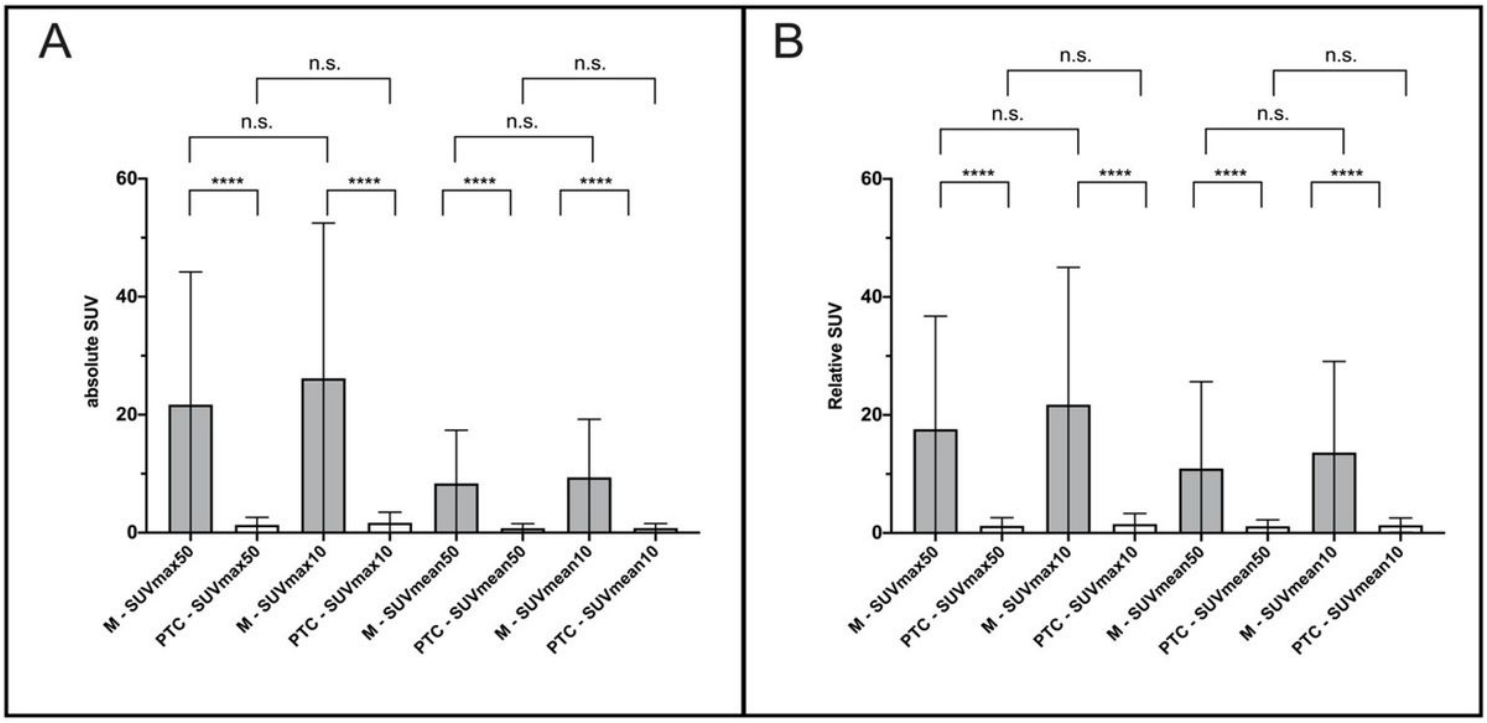

Figure 4

Comparison of meningioma (M, grey bars) and post-treatment-change lesions (PTC, white bars) using maximum and mean SUV acquired over the entire scan period (SUVmax50 and SUVmean50) and the last 10 minutes of acquisition (SUVmax10 and SUVmean10). Shown are mean and standard deviation. Figure 4A demonstrates absolute SUV; Figure 4B demonstrates relative SUV (normalized to the superior sagittal sinus, SSS). Asterisks indicate p-value (****, < 0.0001; n.s., not significant).

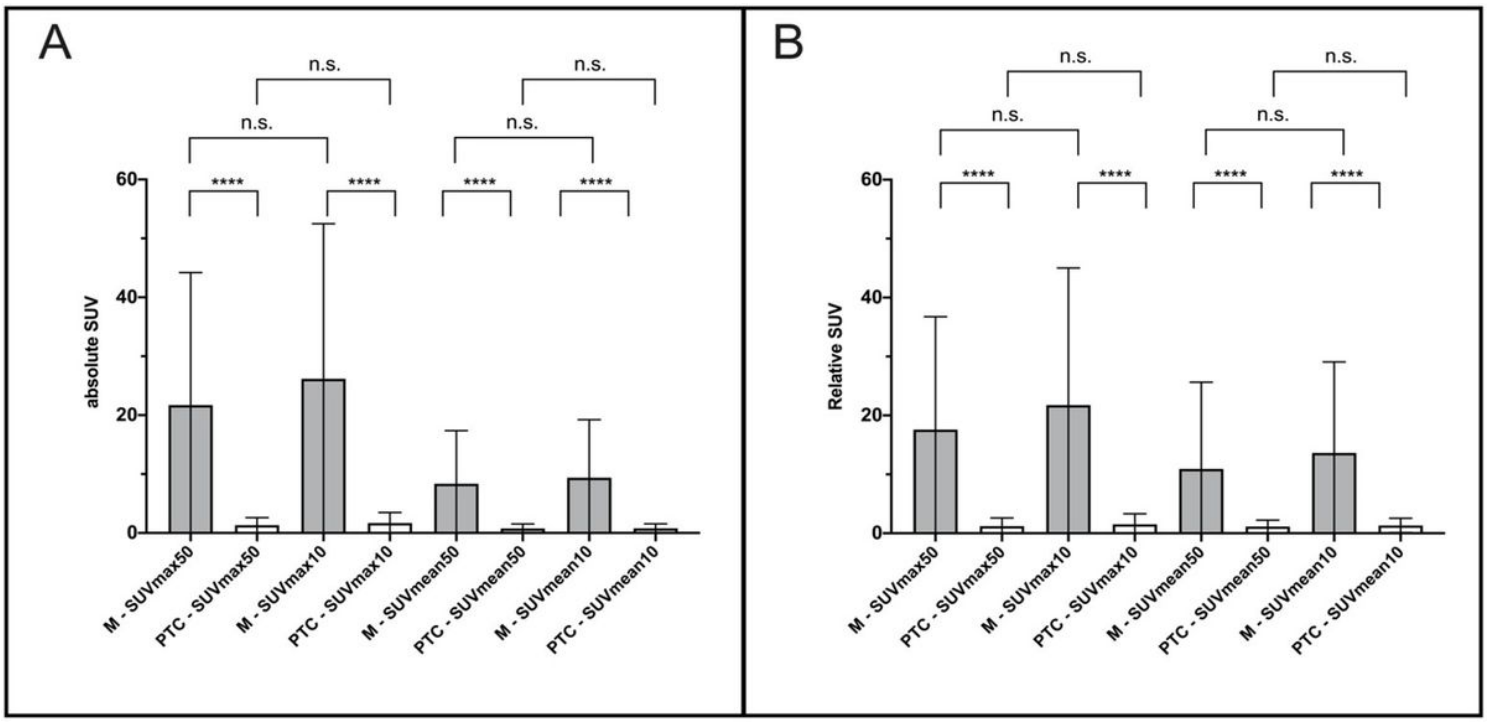

Figure 4

Comparison of meningioma (M, grey bars) and post-treatment-change lesions (PTC, white bars) using maximum and mean SUV acquired over the entire scan period (SUVmax50 and SUVmean50) and the last 10 minutes of acquisition (SUVmax10 and SUVmean10). Shown are mean and standard deviation. Figure 4A demonstrates absolute SUV; Figure 4B demonstrates relative SUV (normalized to the superior sagittal sinus, SSS). Asterisks indicate p-value (****, < 0.0001; n.s., not significant).

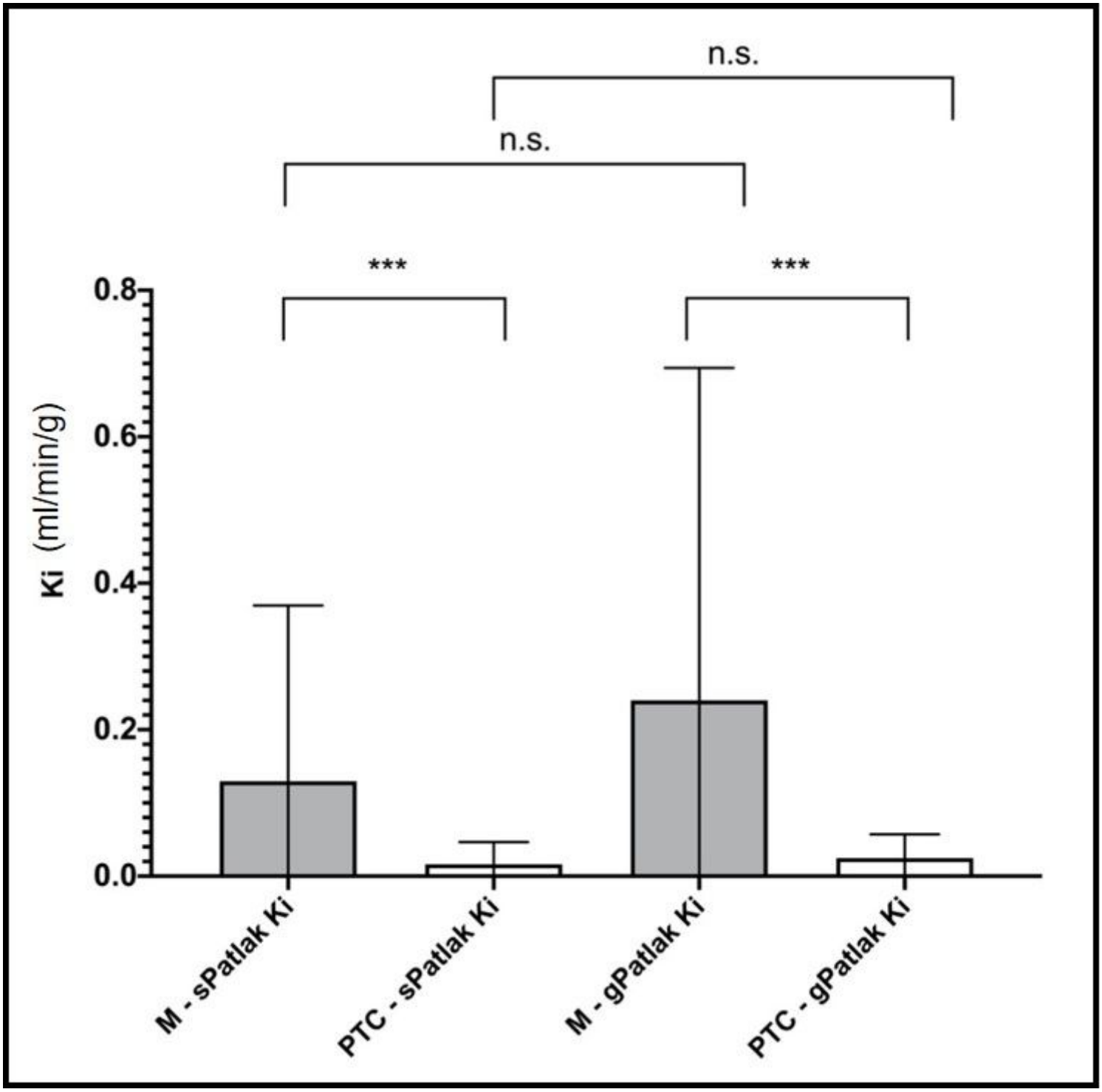

Figure 5

Comparison of meningioma (M, grey bars) and post-treatment-change lesions (PTC, white bars) using sPatlak and gPatlak Ki scores. Shown are mean and standard deviation. Asterisks indicate p-value (***, < 0.001; n.s., not significant).

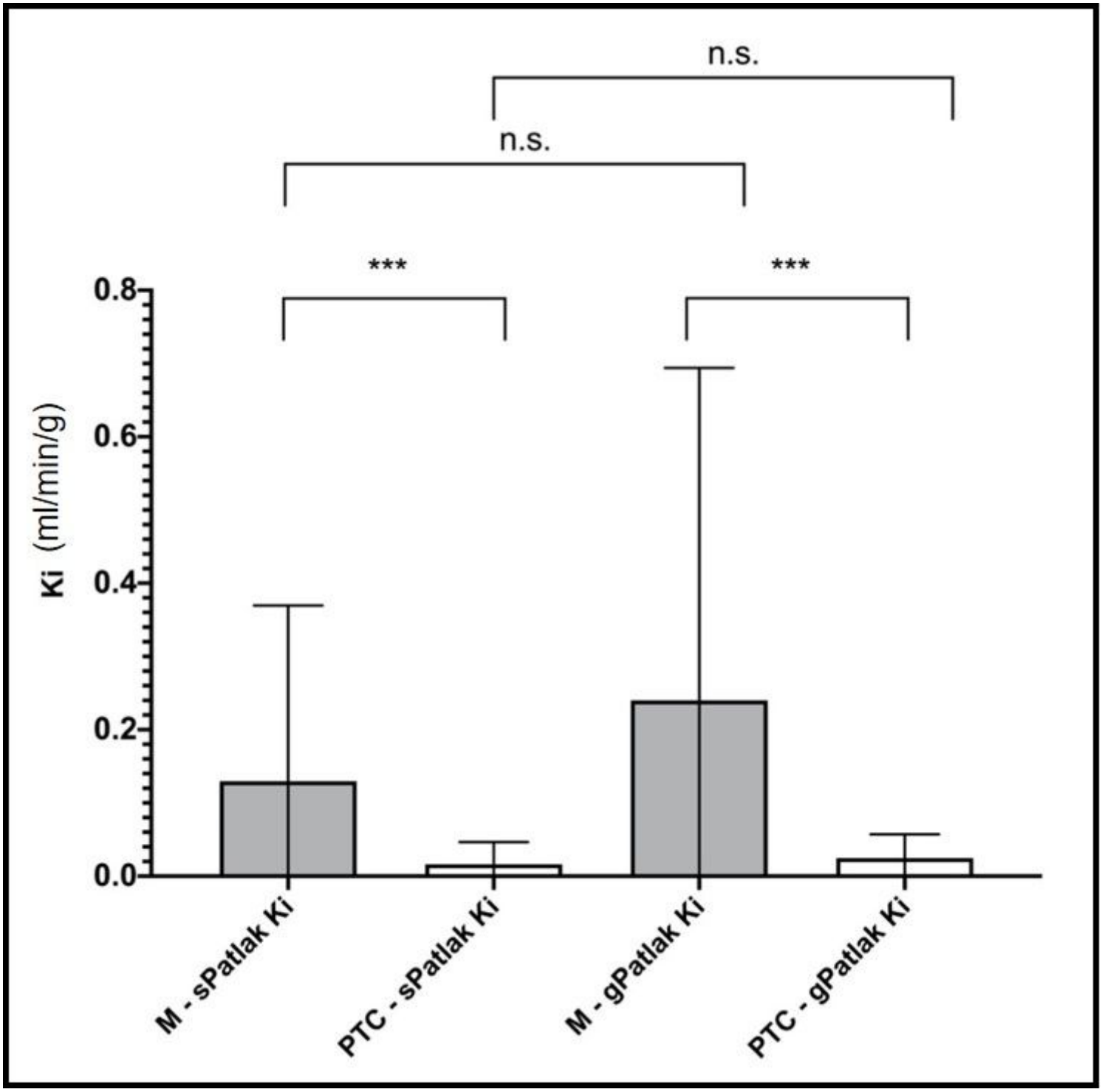

Figure 5

Comparison of meningioma (M, grey bars) and post-treatment-change lesions (PTC, white bars) using sPatlak and gPatlak Ki scores. Shown are mean and standard deviation. Asterisks indicate p-value (***, < 0.001; n.s., not significant).

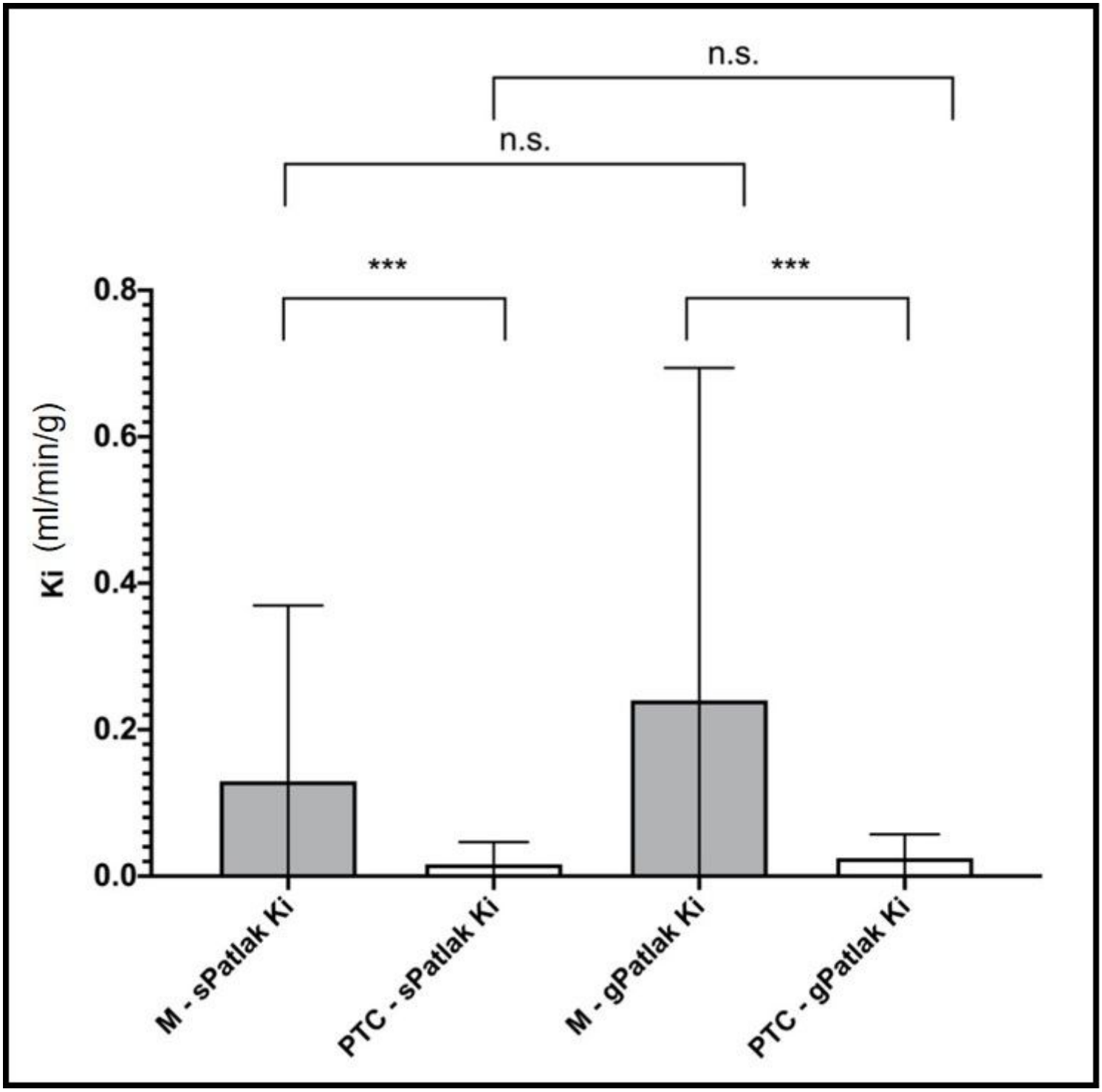

Figure 5

Comparison of meningioma (M, grey bars) and post-treatment-change lesions (PTC, white bars) using sPatlak and gPatlak Ki scores. Shown are mean and standard deviation. Asterisks indicate p-value (***, < 0.001; n.s., not significant).

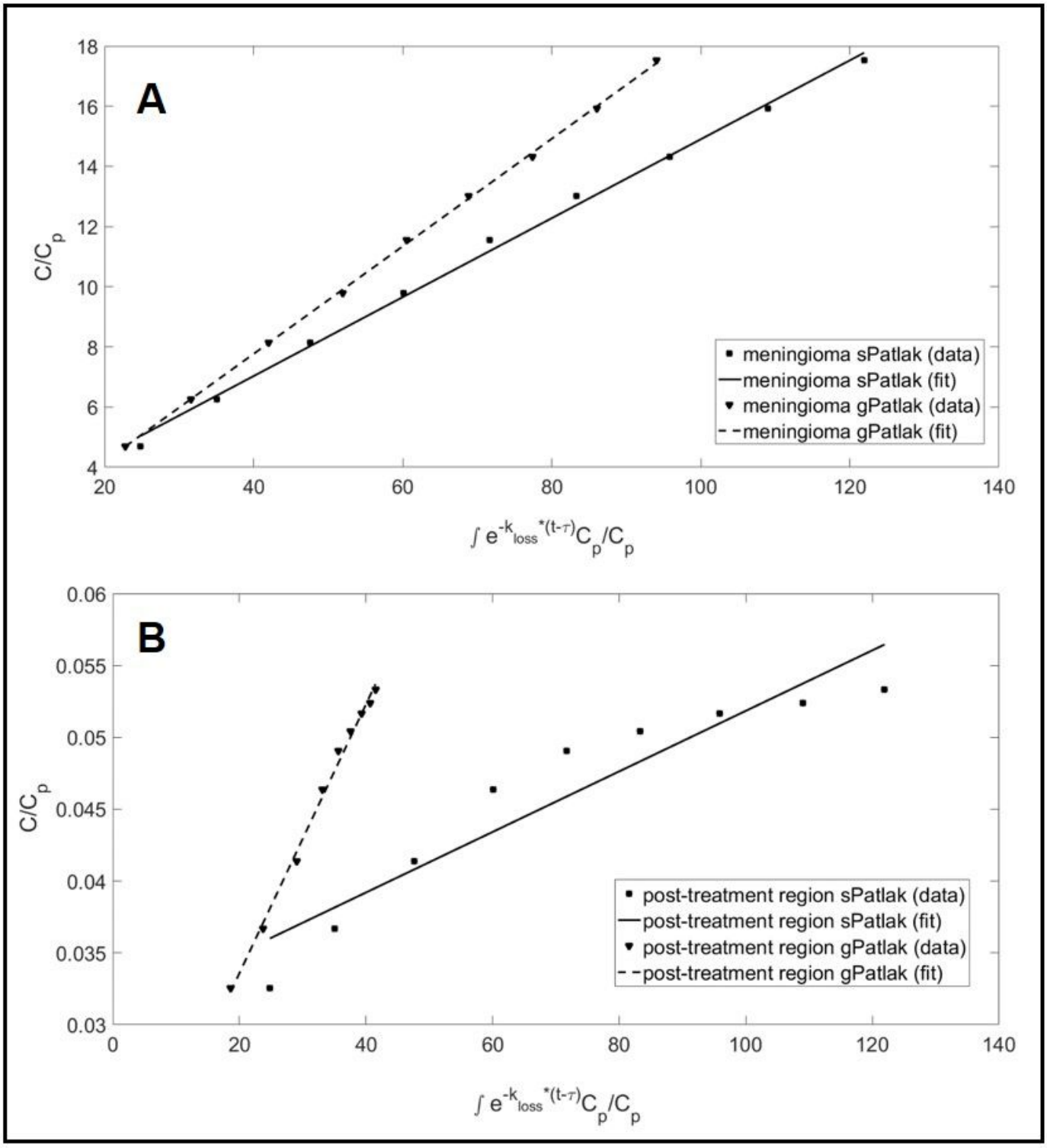

Figure 6

Graphical analysis sPatlak (kloss=0) and gPatlak (kloss≥0) plots of 68Ga-DOTATATE dynamic uptake in a meningioma (A) and post-treatment-change (B) regions from a single subject exam.

Figure 6

Graphical analysis sPatlak (kloss=0) and gPatlak (kloss≥0) plots of 68Ga-DOTATATE dynamic uptake in a meningioma (A) and post-treatment-change (B) regions from a single subject exam.

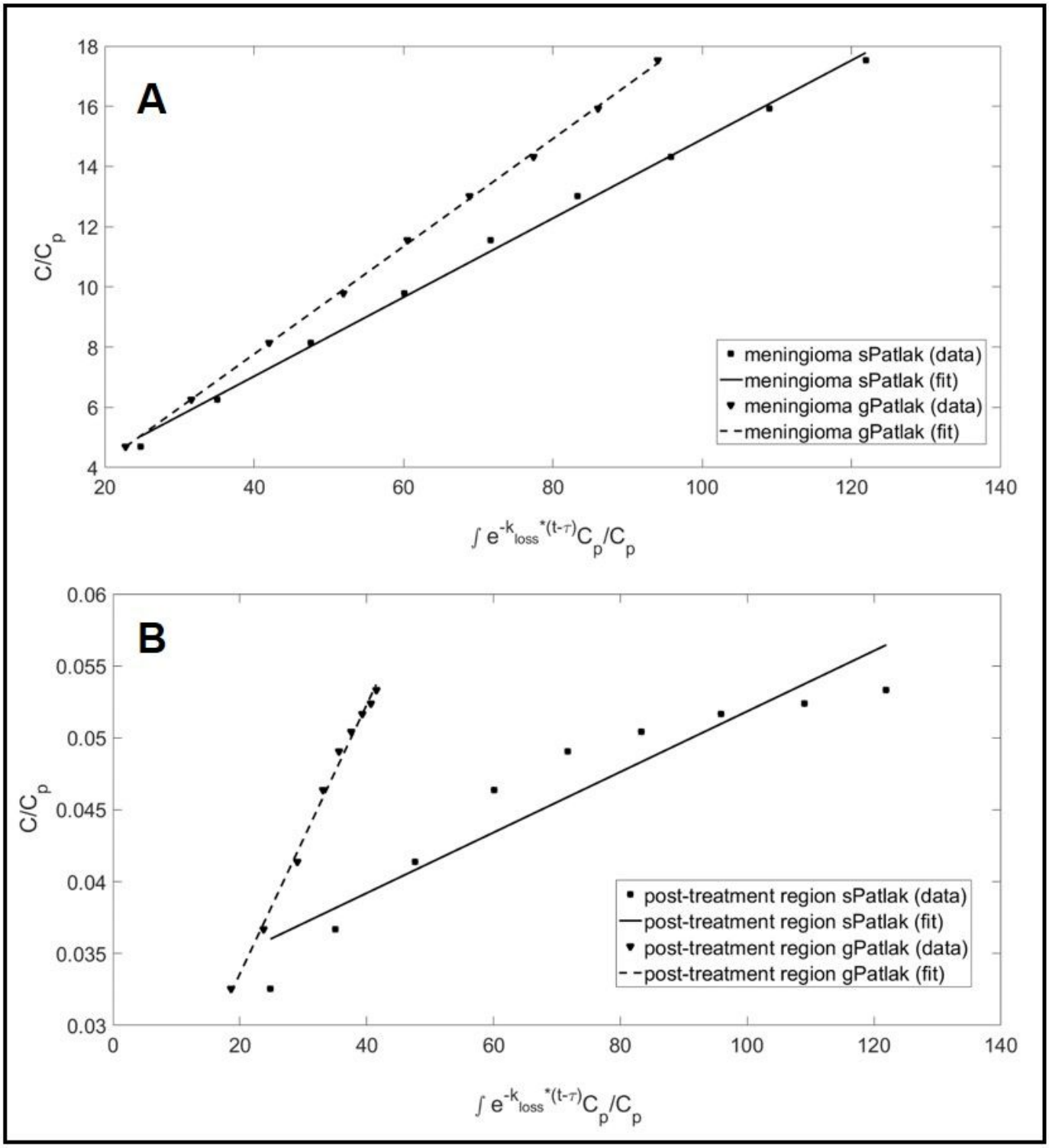

Figure 6

Graphical analysis sPatlak (kloss=0) and gPatlak (kloss≥0) plots of 68Ga-DOTATATE dynamic uptake in a meningioma (A) and post-treatment-change (B) regions from a single subject exam.